IEEE Photonics Journal
An IEEE Photonics Society Publication

Open Access

A Tale of Two Tantalum Borides as Potential Saturable Absorbers for Q-Switched Fiber Lasers

Volume 11, Number 3, June 2019

Haroldo T. Hattori, ***Senior Member, IEEE***
Khalil As'ham
Ahasanul Haque
Ziyuan Li
Benjamin Olbricht

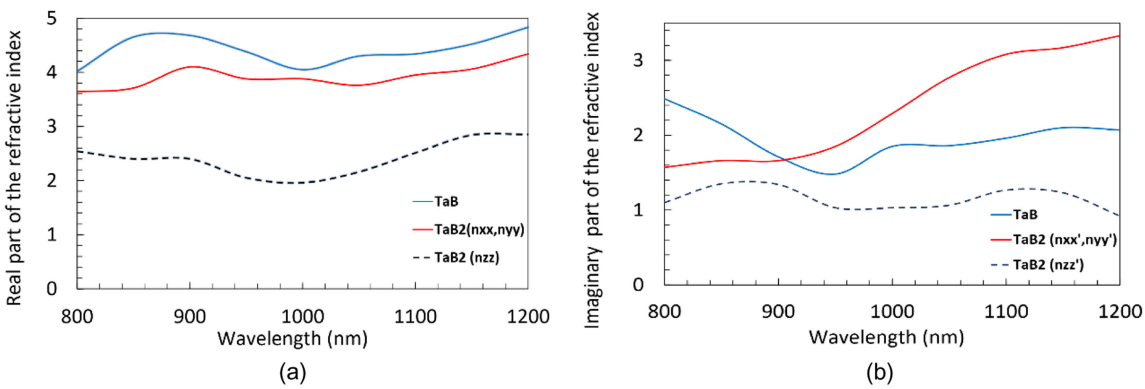

DOI: 10.1109/JPHOT.2019.2906919
1943-0655 © 2019 IEEE

A Tale of Two Tantalum Borides as Potential Saturable Absorbers for Q-Switched Fiber Lasers

Haroldo T. Hattori,[1] ***Senior Member, IEEE***, **Khalil As'ham**,[1] **Ahasanul Haque**,[1] **Ziyuan Li**,[2] **and Benjamin Olbricht**[3]

[1]School of Engineering and Information Technology, UNSW Canberra, Canberra, ACT 2610, Australia
[2]Department of Electronic Materials Engineering, Research School of Physics and Engineering, The Australian National University, Canberra, ACT 2610, Australia
[3]Coupled Optics LLC, Newark, DE 19713 USA

DOI:10.1109/JPHOT.2019.2906919

Manuscript received February 27, 2019; accepted March 19, 2019. Date of publication March 25, 2019; date of current version May 20, 2019. This work was supported in part by the Australian Research Council, in part by the Asian Office of Aerospace Research and Development (AOARD-USAF), and in part by the US Army. Corresponding author: Khalil As'ham (e-mail: k.asham@student.adfa.edu.au).

Abstract: In this paper, we analyze the performance of two tantalum-based boride (*TaB* and TaB_2) microparticles as potential saturable absorbers for high-power fiber lasers. Both materials are ultrahigh temperature ceramics with melting points above 3000 °C, but with different crystalline structures: *TaB* has an orthorhombic structure (nearly isotropic), whereas TaB_2 has a hexagonal structure (uniaxial, anisotropic). Despite their different crystalline structures, the microparticles have a similar low fluence attenuation (between 2.3 and 2.60 dB/μm) and modulation depths (around 2.0 dB/μm), but remarkable different saturation fluences: *TaB* has a saturation fluence of 160 μJ/cm^2, whereas TaB_2 has a saturation fluence of 110 μJ/cm^2. The measured damage thresholds are 112 and 106 mJ/cm^2/pulse for *TaB* and TaB_2, respectively. When incorporated to a fiber laser, the materials produce pulses with durations of 345 ns, lower than those reported by our group in previous papers. The results show that the materials can find potential applications in high-power Q-switched lasers.

Index Terms: Optical fiber lasers, Q-switched lasers, optical materials.

1. Introduction

Q-Switching is a widely known optical technique used to generate short pulses with durations of sub nanoseconds to several milliseconds, which is achieved by controlling the losses in the laser optical cavity [1]. In a Q-switched laser, the initial losses are high, preventing the generation of light while the population is being built-up. However, when the losses are suddenly reduced, the inverted population rapidly decay to lower energy levels, generating high peak power pulses. The generated pulses can be used in different applications such as laser ranging, manufacturing and medicine.

The losses inside the laser cavity can be controlled by either using an external modulator (active Q-switching) or a saturable absorber (passive Q-switching). In case of active Q-switching, the cavity losses can be controlled by using an acousto-optic modulator: the losses remain low when the modulator is turned off, but they can be drastically increased when the modulator deflects the

beam away from the optical cavity [2], [3]. Pulse durations in the order of sub nanoseconds to hundreds of nanoseconds [2], [3] have been reported in the literature by using external modulators.

Another way to produce Q-switched pulses is by adding a saturable absorber to the optical cavity [1], [4]. In a saturable absorber, the material attenuation depends upon the incident energy density (fluence): in typical saturable absorbers, the absorption is high at low fluences and low at high fluences. The losses in a saturable absorber have a non-saturable (linear) component in addition to a nonlinear component which depends upon the incident fluence [4].

Many different saturable absorbers have been reported in the literature, such as Cr^{4+}:YAG [5], [6], semiconductor heterostructures [7]–[10] and CaF_2 [11]. For Cr^{4+}:YAG, pulse durations above 56 ns and energies above 200 mJ have been reported in [5]. In case of semiconductor heterostructures, pulse durations in the order of 56 ps have been reported in the literature [7].

In recent years, two-dimensional materials such as graphene have emerged as potential saturable absorbers for fiber lasers. In case of graphene, atoms are arranged into a two-dimensional honeycomb lattice with a nearest neighbor distance of 1.42 Å and thickness of 0.35 nm [12]. There are many different methods to produce graphene, from mechanical exfoliation [13] to chemical vapor deposition [13]. In addition to its use as saturable absorbers, it can also be used in modulators and photodetectors [14]. Since graphene has a broad absorption spectrum, it has been used in many laser systems including erbium-doped [15]–[17], thulium-doped fibers [18], [19], Er: Y_2O_3 [20] and ytterbium [21], i.e., providing saturable absorption from 1 μm to 3 μm laser systems. Although attractive as a thin saturable absorber, graphene only absorbs $\sim$2.7% per layer [12]. Pulses with durations between 300 ns and 10 μs have been reported in the literature. Carbon nanotubes [22], [23] and few layer black phosphorus [24]–[27] have also been used as saturable absorbers in fiber laser systems.

Another class of emerging materials are the dichalcogenides: they can be exfoliated to two-dimensional layered materials with the layers stacked by weak Van der Waals forces [28]. They are applied in mechanical lubricants, energy storage and electronic/optical devices. In fact, their properties can be tailored by external voltage or stress and they exhibit strong spin-orbital coupling [28]. Transition metal dichalcogenides have been applied to different laser systems [29]–[34] from 635 nm to 3000 nm, with pulse durations from 500 ns to more than 2000 ns. Finally metal nano-particles (e.g., silver and gold) have also been used as saturable absorbers in fiber lasers [35], [36].

Our group has been working on ultrahigh temperature ceramics such as borides for high power (fluence) optical applications [37], [38]. In this manuscript, we report our results on two allotropes of tantalum-based borides: *TaB* and TaB_2. Despite having different chemical compositions, they showed to have similar performance, albeit *TaB* had a somewhat better performance than the other material. The tantalum-based borides have melting temperatures above 3000 °C with different crystalline structures: *TaB* has an orthorhombic crystal structure with lattice constants of 3.295, 8.718 and 3.172 A, while TaB_2 has a hexagonal crystal structure with lattice constants of 3.097 Å and 3.34 Å. Both allotropes are hard materials that can withstand high pressures, with Vickers hardness in the order of 30 GPa. The properties of the borides are dependent on the interaction of *d* orbitals of Tantalum with the *2p* and *2d* boron orbitals [39], [40]. It is predicted that *TaB* will have a slightly lower bulk modulus (288.55 GPa) than TaB_2 (302 GPa).

In this article, the optical properties of *TaB* and TaB_2 are experimentally measured and reported. We show that they have similar losses at lower fluences and similar modulation depth, but *TaB* has a higher saturation fluence than TaB_2. When incorporated into a fiber laser, we observed pulses with duration as short as 345 ns.

2. Theoretical Background and Material Properties

2.1 Initial Theoretical Calculations

To have an estimation of the properties of the different borides, we employ density functional theory and the meta generalized gradient approximation (DFT-MGGA) [41], [42]. The starting point of

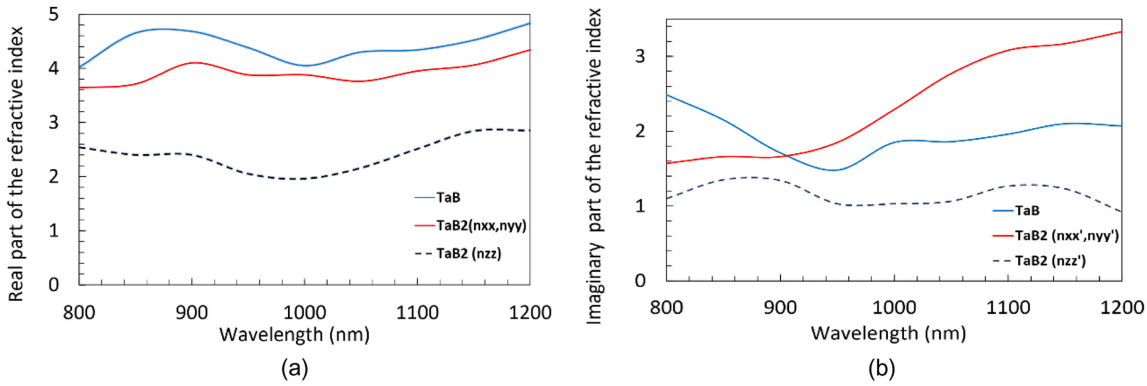

Fig. 1. (a) Real and (b) imaginary parts of the refractive indices of *TaB* and TaB_2. Note that the x-y plane contains the Boron atoms.

DFT-MGGA is to solve the non-interacting auxiliary Schrodinger equation [41], [42],

$$\left[-\frac{h_N^2}{2m_e}\nabla^2 + V_S\right]\varphi_i = \epsilon_i\varphi_i \tag{1}$$

where φ_i is the auxiliary wavefunction for the i^{th} electron in different orbitals, ϵ_i is the auxiliary energy of the i^{th} electron and V_s is the effective single electron potential. The interaction between different electrons are included in V_s.

After minimizing the total energy and determining the auxiliary wavefunctions, the relative electric permittivity is calculated by [41],

$$\varepsilon_{rij}(\omega) = \delta_{ij} - \frac{e^2}{m_e\Omega\omega^2}\sum_k f_k\delta_{ij} + \sum_p \frac{f_k - f_p}{h_N m_e}\frac{\langle\varphi_k|p_i|\varphi_p\rangle\langle\varphi_p|p_j|\varphi_k\rangle}{\epsilon_k - \epsilon_p + \omega - i\eta} \tag{2}$$

where δ_{ij} is the Kronecker delta, i.e., $\delta_{ii} = 1$ and $\delta_{ij} = 0$ if $i \neq j$, Ω is the volume of the unit cell, f_p is the value of the Fermi function at ϵ_p, ω is the radial vacuum frequency (rad/s), η is the damping factor, $p_j = -ih_N\frac{\partial}{\partial x_j}$ is the momentum operator and i, j = x, y, z (note that $x_x = x$, $x_y = y$, $x_z = z$ in the momentum operator).

By using Atomistix software [42], we calculate refractive indices of 4.20 + j1.90, and 2.44 + j3.07 (n_{xx}, n_{yy}) and 3.95 + j1.27 (n_{zz}) for *TaB* and TaB_2, respectively, at the free-space wavelength of 1080 nm (*j* is the imaginary number). In Fig. 1, the plane x-y plane contains the hexagonal arrangement of Boron atoms in TaB_2. Based upon the calculations, we observe that *TaB* is isotropic while TaB_2 is anisotropic (uniaxial). The average refractive index of TaB_2 ($1/3*(n_{xx} + n_{yy} + n_{zz}) = 2.07$, comparable with *TaB*). Compared with noble metals (e.g., silver with a refractive index of 0.238 + i*7.33 at 1080 nm), both materials have lower losses, meaning that their losses lie between noble metals and dielectrics. The polarizability of the materials seems to be confirmed by reference [43], which state that orthorhombic materials (such as *TaB*) can be isotropic while hexagonal structures tend to be anisotropic.

The absorption mechanisms of the tantalum-based borides are explained in different articles [40], [44], [45]: the main absorption comes from the electrons in the tantalum-boride bonds which are stronger than the boron-boron bonds. The tantalum bond has an average length of 2.38 Å [45]. *TaB* has a calculated bandgap of 0.72 eV, i.e., absorbing light at wavelengths lower than 1700 nm, while TaB_2 behaves as a metal, with no bandgap (band diagrams are calculated with Density Functional Theory). As aforementioned, they have different crystalline structures: *TaB* crystallizes in an orthorrombic structure while TaB_2 has a standard hexagonal structure.

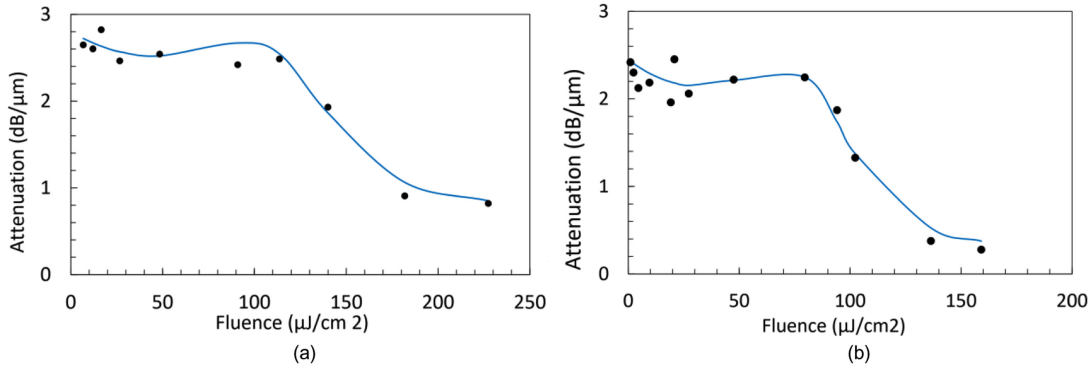

Fig. 2. Measured attenuation of the particles cluster for (a) *TaB* and (b) TaB_2. Data points are fitted through formula (3).

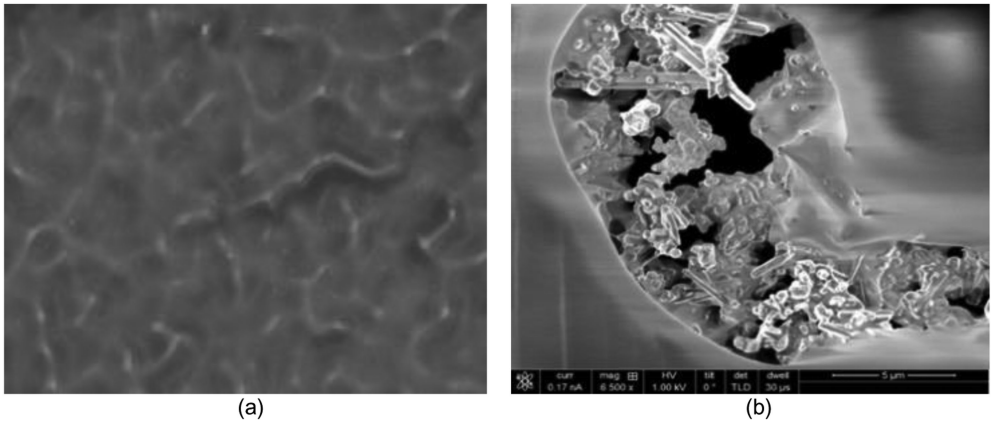

Fig. 3. (a) 100 times magnification of the surface of *TaB*. (b) Damaged *TaB* particles at a fluence of 112 mJ/cm^2/pulse.

2.2 Sample Preparation and Material Measurements

TaB and TaB_2 micro-powder was purchased from *Sigma-Aldrich* company. According to the company website, the average size of the particles is about 44 μm. The particles are then mixed with polyvinyl alcohol (*PVA*) and spin coated at a rotation speed of 500 *rpm* on top of glass slides. The samples are then dried for several minutes, resulting in a deposited layer of about 8 μm. The thickness is measured by using a *Dektak XT* surface profiler, which has a resolution of 10 nm – however the thickness of the materials is non-uniform being thicker at the edges. A commercial Q-switched laser with peak power of 1000 W, operating at 1053 nm and with a spot-size diameter of 2 mm, is used to measure the linear and nonlinear absorbance of the thin-film material. The measured attenuation as a function of the fluence is shown in Fig. 2: it seems that when light is polarized along the *x-y* plane, *TaB* has higher losses than TaB_2. However, the low fluence (energy density attenuation) attenuation is significantly lower than the calculated by *DFT-MGGA*: for example, while *TaB* particles have a low fluence attenuation of 2.8 dB/μm, while the calculated loss is around 96 dB/μm. The enormous discrepancy can be explained by the very non-uniform coating of the glass sample with tantalum boride particles, contamination of the particles by water and *PVA*, and the creation of small areas with no particles. Thin film calculations of borides have shown that *DFT-MGGA* over-estimates the material losses [45] with actual thin-film imaginary refractive indices overestimated by a factor of 2. However, the large discrepancy is mostly due to the non-uniform deposition of the micro-powder solution which strongly scatters light, as explained by *Guineton and co-authors* [46]. In fact, Fig. 3(a) shows a 100 times magnified image of *TaB* surface, showing surface roughness which strongly scatters the incident light.

TABLE 1
Fitted Parameters for the Curves in Fig. 2

Material	*TaB*	TaB_2
Non-saturable attenuation (dB/μm)	0.78	0.27
Saturable attenuation (dB/μm)	2.02	2.18
Saturation fluence (μJ/cm^2)	160	110
Coefficient *a2*	-1.0	-0.95
Coefficient *a3*	-2.45	-2.45
Coefficient *a4*	1.9	0.60
Coefficient *a5*	-1.0	2.5
Coefficient *a6*	4.05	1.0

The absorbance curves can be fit by the formula:

$$\alpha = \alpha_l + \frac{\alpha_{nl}}{1 + \sum_{p=1}^{6} a_p \left[\frac{F}{F_{sat}}\right]^p} \tag{3}$$

where α_l is the linear non-saturable attenuation, α_{nl} is the saturable attenuation, a_p are the fitting coefficients, F is the incident fluence (energy per unit area) and F_{sat} is the saturation fluence. The coefficients were chosen to minimize the mean square error. The coefficient a_1 is close to 1.0, so we keep the typical value of $a_1 = 1.0$. The fitting parameters are shown in Table 1.

Based upon the fitted data, it seems that both materials have similar modulation depth (around 2.0 dB/μm), but *TaB* has a somewhat higher attenuation than TaB_2 at lower fluences: since both materials have similar average imaginary parts of the refractive index and the micro-powder has no defined crystalline orientation, their attenuation should be similar. However, it is evident that TaB_2 has a 30% lower saturation fluence than *TaB*, i.e., the saturation fluences are 110 and 160 μJ/cm^2, respectively. We have tested other borides such as Zirconium boride (ZrB_{12}) [38], which had a saturation fluence of 72 μJ/cm^2 with a modulation depth of 3.0 dB/μm – therefore the tantalum-based borides have lower losses than other materials but higher saturation fluences.

In order to assess the optical damage threshold, experiments with a 1053 nm Q-switched laser with spot-size of 1 mm and maximum fluence of 10 μJ (maximum fluence of 1.27 mJ/cm^2 per pulse) is used to assess the optical damage of the saturable absorbers. At maximum fluence of the commercial Q-switched laser, no optical damage was observed for the samples.

Following the initial experiment, a femtosecond laser (*High Q laser*) operating at the central wavelength of 522 nm with a spot-size diameter of 700 nm is used to characterize the materials further. The laser pulse has duration of 300 fs and it operates at a repetition rate of 20.8 MHz. In a similar experiment performed in [38], the measured damage thresholds are 112 mJ/cm^2/pulse and 106 mJ/cm^2/pulse for *TaB* and TaB_2, respectively – implying that *TaB* can handle a somewhat higher fluence than TaB_2. Fig. 3(b) shows a scanning electron microscope (*SEM*) image of the damaged surface: the figure clearly shows the melting of the micro-particles after the femtosecond laser blast.

The normalized reflected pulses for both materials are shown in Fig. 4(a): the broader reflected pulse response is for *TaB*. Fitting the pulse rise times by (1-exp(-(t-t_{in})/τ_s) where τ_s is the saturation lifetime and the pulse decay by K_1 exp(-(t-t_1)/τ_{r1}) + K_2 exp(-(t-t_2)/ τ_{r2}), we obtain $\tau_s = 80$ ps and 30 ps, $\tau_{r1} = 43.3$ ps and 23.64 ps, and $\tau_{r2} = 289.4$ ps and 248.8 ps for *TaB* and TaB_2, respectively. It is clear that T*aB* has a slower response to the incident pulse than TaB_2.

The Raman spectra for *TaB* (solid line) and TaB_2 (dashed line) are also measured and the results presented in Fig. 4(b): there is a broad peak at 1355 cm^{-1}, which is similar to the presented by *Nyquist and Kagel* [47]. However, there is also a stronger Raman peak at 1309 cm^{-1} for TaB_2 which seems to reflect the vibrations the additional *TaB* covalent bond in the tantalum diboride when compared with tantalum boride (1:1).

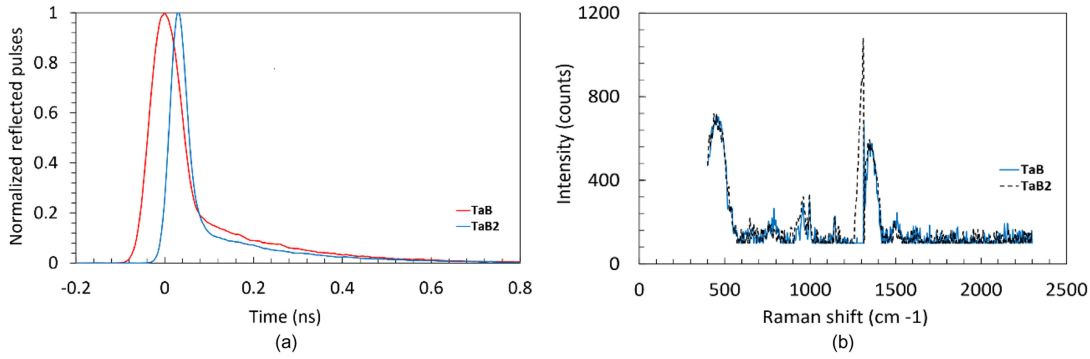

Fig. 4. (a) Normalized reflected pulses for *TaB* and TaB_2 – *TaB* has a broader response than TaB_2. (b) Raman spectrum for *TaB* (solid line) and TaB_2 (dashed line).

TABLE 2
Parameters for Different Materials

Material	Low power absorptance	High power absorptance	Saturation fluence/power density	Damage fluence	Ref.
Graphene	2.3 % per layer	0.77 % per layer	0.53 MW/cm^2	57 mJ/cm^2	[14,47]
BP (few layers)	14.3 %	13.8%	6.9 MW/cm^2	N/A	[23]
$MoTe_2$ (few layers)	11 %	4%	18 MW/cm^2	N/A	[33]
SESAM	2 %	0.5%	50 μJ/cm^2	30 mJ/cm^2	[8]
ReS_2 (few layers)	9%	7%	0.8 mJ/cm^2	N/A	[31]
ZrB_{12}	3.6 dB/μm	0.05 dB/μm	72 μJ/cm^2	132 mJ/cm^2	[37]
TaB	2.8 dB/μm	0.7 dB/μm	160 μJ/cm^2	112 mJ/cm^2	This work
TaB_2	2.45 dB/μm	0.27 dB/μm	110 μJ/cm^2	106 mJ/cm^2	This work

2.3 Comparison of Saturable Absorbers

Table 2 compares the parameters of different bulk and two-dimensional materials – albeit different articles provide either only saturation fluence or saturation power density. Based upon reported data, ZrB_{12} seems to have the highest damage fluence, with similar damage fluence to *TaB* and TaB_2 – in fact, borides have significantly higher damage thresholds than other materials such as graphene and SESAM. Both tantalum-based borides have higher saturation fluences than SESAM (TaB_2 nearly two times and *TaB* nearly three times higher saturation fluences).

Although it is hard to compare different materials, the borides have higher absorptances than the two-dimensional materials and higher modulation depths: graphene can have a 66% modulation depth, while *TaB* has a 75% modulation depth, TaB_2 has 89% modulation depth and ZrB_{12} has a 99% modulation depth. By comparison, dichalcogenides do not have large modulation depths.

3. Experiments With a Fiber Laser

To incorporate the borides to the fiber laser, we initially remove the jacket from some fiber pieces. The passive fiber used in our experiments is a *SM* 980-5.8 fiber from *Thorlabs*, with a spot-size diameter of 5.8 μm, and a cladding diameter of 125 μm. The cladding is removed by using a 24% solution of hydrofluoric acid (HF) for 2 hours and 20 minutes, leading to a remaining fiber diameter of 12 μm. After the removal of the cladding, boride micro-particles are then mixed with PVA and deposited on top of the clad less fiber sections. After water evaporates and PVA solidifies, it keeps the micro-particles close to the fiber core. We estimate that, for a 10 cm fiber section, the low fluence attenuation is in the order of 6 dB.

The schematic of the fiber laser is shown in Fig. 5(a), with the photograph of the constructed fiber laser shown in Fig. 5(b). The ring fiber laser is pumped by a 980 nm *cw* laser with a maximum power of 2.2 W. The pump laser can be externally modulated by a signal generator at a maximum

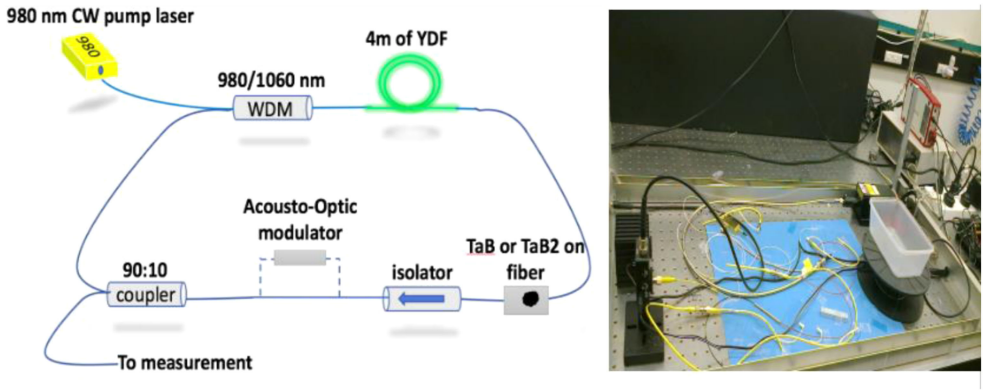

(a) (b)

Fig. 5. (a) Schematic of the ring ytterbium doped fiber laser. (b) Photograph of the actual laser.

TABLE 3
Long Term Stability

Period (day)	Narrowest pulse duration (ns)	Output Power (mW)
0	345	200
15	320	180
30	300	215
45	360	190

repetition rate of 1 kHz. The pump light is then injected into a 980/1060 nm *WDM* coupler (with a 3-dB loss) that protects the pump laser from potential reflected light from the ring laser, while allowing the circulation of the emitted light through the ring – therefore, the maximum effective pump power is around 1.1 W. The pump power then goes through 4m of ytterbium doped fiber, *YB 1200-6/125 DC* which is the active medium for the fiber laser. The 90:10 coupler allows that 10% of the circulating power to reach either a power meter, a fast detector or a spectrum analyzer.

A tellurium dioxide acousto-optic modulator from *Gooch-Housego* company can be added to the ring laser as shown in Fig. 5(a): the acousto-optic modulator is driven by a radio-frequency signal at 150 MHz which can be turned on-off at different repetition rates. The addition of the modulator allows changing the repetition rate from hundreds of hertz to 1 MHz, albeit bringing an additional 2 dB loss to the ring laser. The acousto-optic modulator also partially halts the circulation of light through the ring (when it is turned off), reducing the effects of dispersion through round trips around the fiber ring [2]. Since we have obtained similar results for both *TaB* and TaB_2, we will emphasize the results for *TaB*, unless when we need to highlight the performance difference between the two materials.

3.1 Long Term Stability

Tests were conducted with the saturable absorbers over more than 1.5 months: during this period, no major degradation was observed in the performance of the saturable absorbers in the fiber laser as shown in Table 3. We have also run long continuous testing over 3 days and the laser presented very similar characteristics: we believe that the saturable absorbers can withstand long term illumination.

3.2 Stand-Alone Tantalum Based Saturable Absorbers

In the first experiment, no acousto-optic modulator is employed, and the 980 nm pump laser is not externally modulated, i.e., the optical fiber ring is driven by a cw signal. Under *cw* Q-switching, a series of pulses are observed with a variable repetition period ranging from 7 μs to 60 μs. The laser

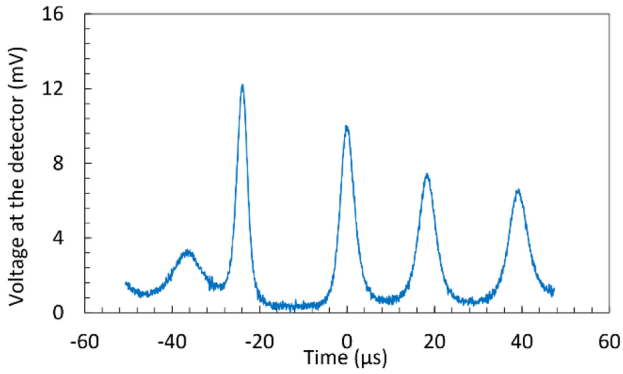

Fig. 6. Example of continuous wave Q-switched pulse.

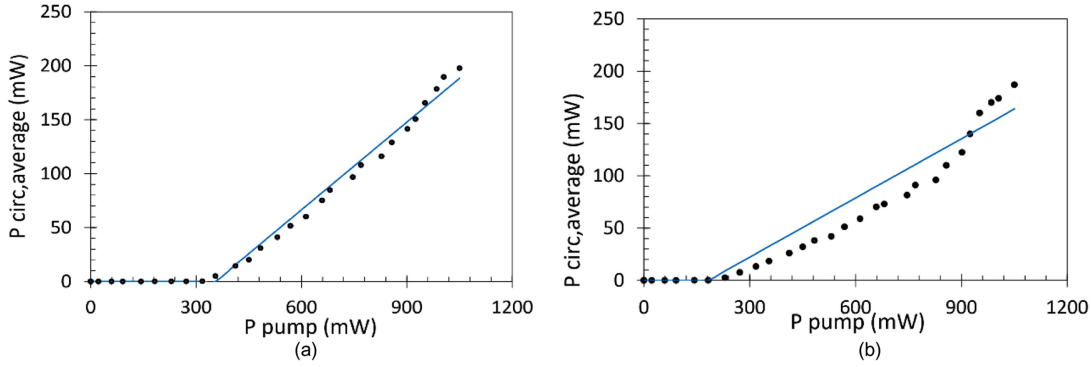

Fig. 7. Average circulating power as a function of the peak power for (a) *TaB* and (b) TaB_2.

emission spectrum is centered at 1073 nm with a linewidth of about 8 nm. Fig. 6 shows a typical sequence of cw pulses at a pump power of 400 mW for TaB_2.

The laser is then externally modulated at a repetition rate of 1 kHz, with a 50% duty cycle, unless otherwise stated. The average circulating powers (P_{circ}) as a function of the peak pump power (P_{pump}, including the 3 dB losses of the coupler) are shown in Figs. 7(a) (*TaB*) and 7(b) (TaB_2). It is interesting to note that both lasers have similar performance, with similar threshold pump powers (around 380 mW) and similar slope (40 mW of circulating power change for a 620 mW of differential pump power) – this is somewhat expected by the fact that both materials have similar average losses.

Fig. 8(a) shows a typical periodic sequence of Q-switched pulses for *TaB* when the pump laser is modulated at a repetition rate of 1 kHz and duty cycle of 27%. The voltage at the detector changed from 1.88 mV to a maximum of 2.88 mV reflecting a variation in the power of the pulses by around 50%. In general, single pulses per period are clearly observed at low powers for a duty cycle of 50% but multiple pulses per period start to appear at higher pump powers as reported in previous papers [e.g., 37], but the multiple pulses can be eliminated by reducing the duty cycle of the pump power.

A spectral analyzer is used to measure the emission spectrum of the constructed laser: the power spectrum analyzer measures the filtered power through a diffraction grating and the diffracted spectral lines are imaged through a charge-coupled (*CCD*) camera. The analyzer then adds up all measured values and normalizes the spectrum. The power spectrum density (*PSD*) is therefore a normalized version of the real power spectrum. However, the emission spectrum is centered at 1075 nm with a linewidth of 4 nm, as shown in Fig. 8(b).

Fig. 9(a) shows a typical pulse at the pump power of 850 mW for *TaB*. The pulse duration is about 360 ns, shorter than any previously reported results from our group on *borides* [37], [38] and MnO_2 [49]. The full width at half maximum (*FWHM)* as a function of the peak pump power

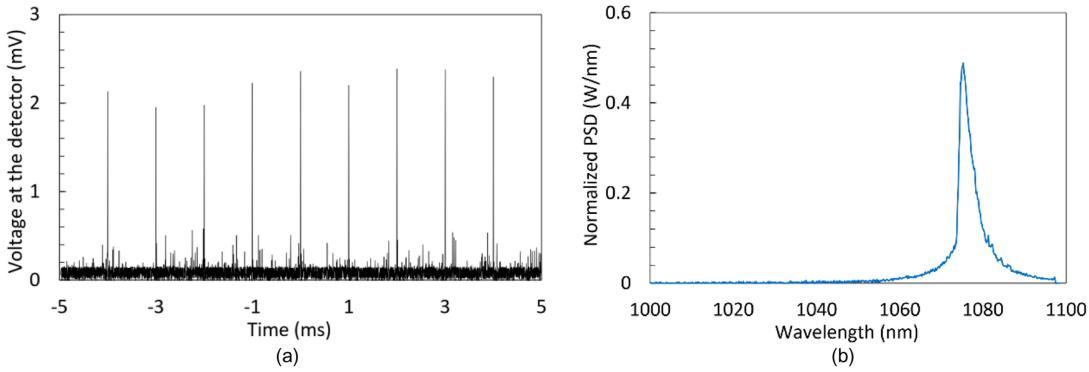

Fig. 8. (a) Typical sequence of pulses for a repetition rate of 1 kHz, but in this case at maximum pump power and a duty cycle of 27%. (b) Typical emission spectrum for this sequence of pulses at a repetition rate of 1 kHz. Note that there is no acousto-optic modulator in the loop and the pump laser is directly modulated at 1 kHz. The saturable absorber is *TaB*.

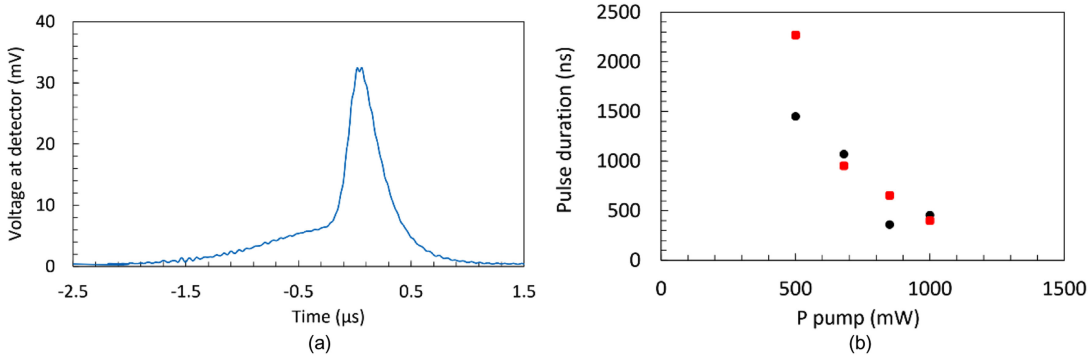

Fig. 9. (a) Pulse duration at a pump power of 850 mW. (b) Pulsed duration as a function of the pump power for *TaB* (black, circular markers) and TaB_2 (red, square markers).

for *TaB* (black and circular markers) and TaB_2 (red, square markers) are shown in Fig. 8(b). At the maximum pump power of our laser system, the pulse duration for *TaB* and TaB_2 are 460 ns and 400 ns, respectively. The longer pulse duration at 500 mW for TaB_2 can be explained by the higher threshold pump power for TaB_2, nonetheless, they seem to have similar performance, with a slightly better performance and generation of more stable pulses for *TaB*. At a peak pump power of 1 W and repetition rate of 1 kHz, the average power is 200 mW leading to an energy of 200 μJ. Since the pulse duration is about 400 ns, the peak power of the emitted pulse is about 500 W.

3.3 Addition of Acousto-Optical Modulator to the Ring

To better assess the properties of the laser, an acousto-optic modulator is added to the laser loop: although it adds a 2 dB loss to the laser cavity, it allows the laser to work at higher repetition rates. For example, Fig. 10(a) shows the pulse at a repetition rate of 10 kHz: the pulse duration is about 355 ns, close to the obtained with no acousto-optic modulator. It seems that the pulse duration of 360 ns is the shortest duration that we can obtain with our system and is reproducible at different repetition rates. The emission spectrum of this pulse is shown in Fig. 10(b): it is again centered at 1075 nm but with a linewidth of 6 nm. The peak power is reduced in this case because of the acousto-optic modulator loss to about 3.6 W.

A different laser dynamic occurs at a 1 kHz repetition rate with the addition of the acousto-optic modulator. At this repetition rate, we can observe Q-switching mode-locking as shown in Fig. 11(a):

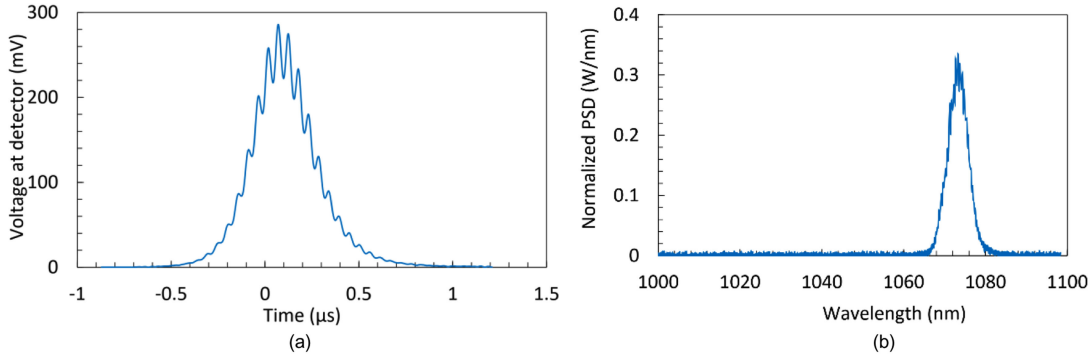

Fig. 10. (a) Pulse at a pump power of 1050 mW. (b) Emission spectrum of the pulses.

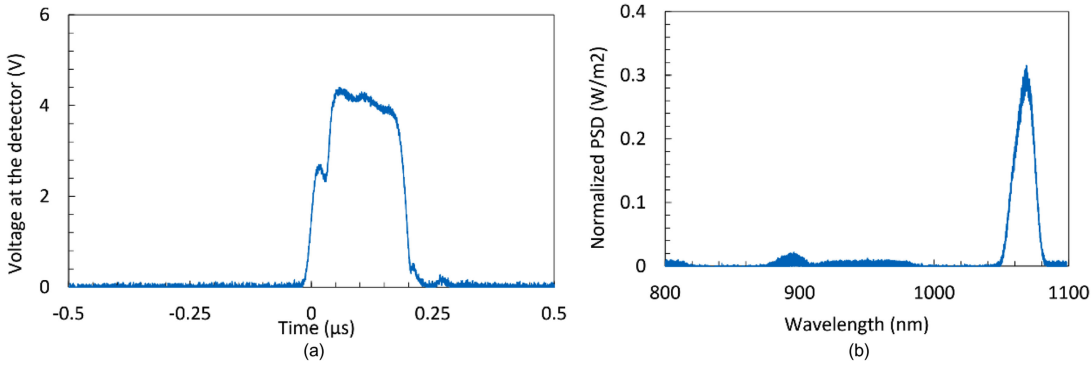

Fig. 11. (a) Pulse at a pump power of 1050 mW with the acousto-optic modulator and *TaB* as saturable absorber and (b) its emission spectrum.

the pulse is further shortened to a duration of 194 ns and the emission spectrum broadens as shown in Fig. 11(b). The emission spectrum is still centered at 1075 nm, but lateral sidelobes start to appear at other wavelengths (e.g., 900 nm).

Although we reached the maximum pump power before full mode-locking occurs – however if the pump power is further increased, the emission spectrum would be broadened and the pulses will be shortened due to the coupling between the modes in the laser cavity [1], [37].

3.4 Comparison With Different Laser Systems

The performance of the proposed saturable absorbers *TaB* and TaB_2 are compared with the performance of different saturable absorbers such as graphene, black phosphorus, carbon nanotube, dichalcogenides (e.g., MoS_2) and SESAM in different laser systems. The comparison for ring lasers is shown in Table 4. From Table 4, it is clear that by using *TaB* and TaB_2, we are able to achieve the lowest pulse widths, the highest output power, and, therefore, the highest pulse energy compared with the other materials. It can also be observed that TaB_2 can produce narrower light pulses than *TaB*. Furthermore, when an acousto-optic modulator integrated inside the cavity, even shorter pulse width can be obtained. Those results indicate that the proposed laser system is very promising light source for many industrial applications where high pulse energy is highly demanded.

In the literature, shorter pulses have been reported with Fabry-Perot cavities as shown in Table 5. This is expected become Fabry-Perot lasers have shorter cavity lengths that will lead to shorter pulses [50] and, in addition, fiber dispersion leads to longer pulses in a ring cavity [2]. However, since *TaB* and TaB_2 are ultrahigh temperature ceramics, they can eventually generate higher energy pulses than other commonly used saturable absorbers.

TABLE 4
Comparison of Ring Q-Switched Laser Using Different Saturable Absorber Materials

Material	Operating wavelength (μm)	Min pulsewidth (μs)	Max output average power (mW)	Max pulse energy	Ref.
Graphene	1.094	3.5 - 15	130	18.8 nJ	[16,21]
Black phosphorus	1.038 – 1.083	1.16 - 4	8.45	2.9 - 7.1 nJ	[24,26]
MoS_2	1.027	1.3	25	141.8 nJ	[33]
TaB	1.075	0.46 (Stand Alone) 0.36 (acousto-optic)	200	200 μJ	This work
TaB_2	1.075	0.4 (Stand Alone) 0.31 (acousto-optic)	200	200μJ	This work

TABLE 5
Comparison of Fabry-Perot Q-Switched Laser Using Different Saturable Absorber Materials

Material	Operating wavelength (μm)	Min pulsewidth (ns)	Max output average power (w)	Max pulse energy (μJ)	Ref.
Graphene	1.123	875	0.332	7.09	[20]
Black phosphorus	1.046	119	1.23	~1.7	[25]
SESAM	1	10-2000	0.317	6.65	[7]

4. Conclusions

In this article, we have assessed the properties of 2 allotropes of tantalum boride: *TaB* and TaB_2. *TaB* seems to be an isotropic material while TaB_2 is anisotropic. The micro-particles have an attenuation between 2.3 and 2.6 dB/μm and a modulation depth of about 2.0 dB/μm. The saturation fluence for *TaB* and TaB_2 are 160 μJ/cm^2 and 110 μJ/cm^2, respectively. *TaB* has a slower response than TaB_2 as evidenced by our femtosecond laser experiments, while they have similar damage thresholds.

When incorporated to a fiber laser, the saturable absorbers produced pulses as short as 360 ns, the shortest pulses that we have obtained with other materials using the same setup. Since these materials have high melting temperatures, they can find potential applications in high power pulsed lasers.

References

[1] A. E. Siegman, *Lasers*. Stanford, CA, USA: Univ. Sci. Books, 1986.
[2] H. T. Hattori and A. Khaleque, "Finite-difference time-domain methods to analyze ytterbium-doped Q-switched fiber lasers," *Appl. Opt.*, vol. 55, pp. 1649–1657, 2016.
[3] M. Delgado-Pinar, D. Zalvidea, A. Díez, P. Pérez-Millán, and M. V. Andrés, "Q-switching of an all-fiber laser by acousto-optic modulation of a fiber Bragg grating," *Opt. Exp.*, vol. 14, pp. 1106–112, 2006.
[4] R. Paschotta, *RP* Photonics Encyclopedia. [Online]. Available: hhtp://www.rp-photonics.com
[5] X. Zhang, A. Brenier, J. Wang, and H. Zhang, "Absorption cross-sections of Cr^{4+}:YAG at 946 nm and 914 nm," *Opt. Mater.*, vol. 26, pp. 293–296, 2004.
[6] S. Forget *et al.*, "Passively Q-switched diode-pumped Cr4+:YAG/Nd^{3+}:$GdVO_4$ monolithic microchip laser," *Opt. Commun.*, vol. 259, pp. 816–819, 2006.
[7] U. Keller *et al.*, "Semiconductor saturable absorber mirrors (SESAM's) for femtosecond to nanosecond pulse generation in solid-state lasers," *IEEE J. Sel. Topics Quantum Electron.*, vol. 2, no. 3, pp. 435–453, Sep. 1996.
[8] C. J. Saraceno *et al.*, "SESAMs for high-power oscillators: Design guidelines and damage thresholds," *IEEE J. Sel. Topics Quantum Electron.*, vol. 18, no. 1, pp. 29–41, Jan./Feb. 2012.
[9] R. Paschotta and U. Keller, "Passive mode locking with slow saturable absorbers," *Appl. Phys. B*, vol. 73, pp. 653–662, 2001.
[10] M. Wang *et al.*, "Passively Q-switched Er-doped fiber laser using a semiconductor saturable absorber," *Optik*, vol. 125, pp. 2154–2156, 2014.
[11] L. Su *et al.*, "Passively Q-switched Yb3+ laser with Yb3+-doped CaF2 crystal as saturable absorber," *Opt. Exp.*, vol. 15, pp. 2375–2379, 2007.
[12] M. I. Kastnelson, *Graphene: Carbon in Two-Dimensions*, Cambridge UK: Cambridge Univ. Press, 2012.
[13] U. Yorulmaz, A. Özden, N. K. Perkgöz, F. Ay, and C. Sevik, "Vibrational and mechanical properties of single layer MXene structures: A first-principles investigation," *Nanotechnology*, vol. 27, 2016, Art. no. 335702.

[14] S. C. Dhanabalan, J. S. Ponraj, H. Zhang, and Q. Bao, "Present perspectives of broadband photodetectors based on nanobelts, nanoribbons, nanosheets and the emerging 2D materials," *Nanoscale*, vol. 8, pp. 6410–6434, 2016.
[15] Q. Bao *et al.*, "Atomic-layer graphene as saturable absorber for ultrafast pulsed laser," *Adv. Funct. Mater.*, vol. 19, pp. 3077–3083, 2009.
[16] Z. T. Wang, Y. Chen, C. J. Zhao, H. Zhang, and S. C. Wen, "Switchable dual-wavelength synchronously Q-switched erbium-doped fiber laser based on graphene saturable absorber," *IEEE Photon. J.*, vol. 4, no. 3, pp. 879–886, Jun. 2012.
[17] H. Ahmad, F. D. Muhammad, M. Z. Zulkifli, and S. W. Harun, "Graphene oxide based saturable absorber for all-fiber Q-switching with a simple optical deposition technique," *IEEE Photon. J.*, vol. 4, no. 6, pp. 2205–2212, Dec. 2012.
[18] H. Ahmad, A. Z. Zulkifli, K. Thambiratnam, and S. W. Harun, "2.0 μm Q-switched thulium-doped fiber with graphene oxide saturable absorber," *IEEE Photon. J.*, vol. 5, no. 4, Aug. 2013, Art. no. 1501108.
[19] B. Lu, H. Chen, M. Jiang, X. Chen, Z. Ren, and J. Bai, "Graphene-based passive Q-switching for a 2 μm thulium doped fiber laser," *Laser Phys.*, vol. 23, 2013, Art. no. 045111.
[20] X. Guan *et al.*, "Continuous-wave and chemical vapor deposition graphene-based passively Q-switched Er:Y_2O_3 ceramic lasers at 2.7 μm," *Appl. Opt.*, vol. 57, pp. 371–376, 2018.
[21] L. Liu, H. T. Hattori, E. G. Mironov, and A. Khaleque, "Composite chromium and graphene oxide as saturable absorber in ytterbium-doped Q-switched fiber lasers," *Appl. Opt.*, vol. 53, pp. 1173–1180, 2014.
[22] N. Kasim, A. H. H. Al-Masoodi, F. Ahmad, Y. Munajat, H. Ahmad, and S. W. Harum, "Q-switched ytterbium-doped fiber laser using multi-walled carbon nanotubes saturable absorber," *Chin. Opt. Lett.*, vol. 12, 2014, Art. no. 031403.
[23] T. Han *et al.*, "Nanotube-polymer composites for ultrafast photonics," *Adv. Mater.*, vol. 21, pp. 3874–3897, 2009.
[24] F. Rashid *et al.*, "Using black phosphorus saturable absorber to generate dual wavelengths in a Q-switched ytterbium-doped fiber laser," *Laser Phys. Lett.*, vol. 13, 2016, Art. no. 085102.
[25] J. Ma *et al.*, "Few-layer black phosphorus based saturable absorber mirror for pulsed solid-state lasers," *Opt. Exp.*, vol. 23, pp. 22643–22648, 2017.
[26] Z. Qin *et al.*, "Black phosphorus Q-switched and mode-locked mid-infrared Er:ZBLAN fiber laser at 3.5 μm wavelength," *Opt. Exp.*, vol. 7, pp. 8224–8231, 2018.
[27] Z. Qin *et al.*, "Black phosphorus Q-switched and mode-locked mid-infrared Er:ZBLAN fiber laser at 3.5 μm wavelength," *Opt. Exp.*, vol. 7, pp. 8224–8231, 2018.
[28] Z. M. Wang, *MoS2 Materials, Physics and Devices*, Heidelberg, Germany: Springer, 2014.
[29] D. Wu, Z. Guo, J. Peng, J. Weng, Z. Cai, and H. Xu, "Size effect of WSe_2 on red passively Q-switched fiber laser output performance," *Appl. Opt.*, vol. 57, pp. 4955–4959, 2018.
[30] H. Ahmad *et al.*, "Mixed transition metal dichalcogenide as saturable absorber in ytterbium, praseodymium, and erbium fiber laser," *IEEE J. Quantum Electron.*, vol. 54, no. 3, Jun. 2018, Art. no. 1600409.
[31] B. Yan *et al.*, "Bilayer platinum diselenide saturable absorber for 2.0 μm passively Q-switched bulk lasers," *Opt. Exp.*, vol. 28, pp. 31657–31663, 2018.
[32] M. Fan *et al.*, "Continuous wave and ReS_2 passively Q-switched Er:SrF_2 laser at $\sim$3 μm," *Opt. Lett.*, vol. 43, pp. 1726–1729, 2018.
[33] R. Woodward *et al.*, "Tunable Q-switrched fiber laser based on saturable edge state absorption in few layer molybdenum disulfide (MoS_2)," *Opt. Exp.*, vol. 22, pp. 31113–31122, 2014.
[34] Y. Zhang *et al.*, "$MoTe_2$-based broadband wavelength tunable eye-safe pulsed laser source at 1.9 μm," *IEEE Photon. Technol. Lett.*, vol. 30, no. 21, pp. 1890–1893, Nov. 2018.
[35] C. Pang *et al.*, "Tailoring optical nonlinearities of $LiNbO_3$ crystals by plasmonic silver nanoparticles for broadband saturable absorbers," *Opt. Exp.*, vol. 26, pp. 31276–31289, 2018.
[36] W. Duan *et al.*, "Passively Q-switched mid-infrared laser pulse generation with gold nanospheres as a saturable absorber," *Opt. Lett.*, vol. 43, pp. 1179–1182, 2018.
[37] M. Morshed, H. T. Hattori, A. Haque, and B. C. Olbricht, "Magnesium diboride (MgB_2) as a saturable absorber for a ytterbium-doped Q-switched fiber laser," *Appl. Optics*, vol. 56, no. 27, pp. 7611–7617, 2017.
[38] H. T. Hattori, A. Haque, B. C. Olbricht, "Zirconium boride as a high fluence saturable absorber for Q-switched fiber lasers," *IEEE Photon. Technol. Lett.*, vol. 30, no. 1, pp. 11–14, Jan. 2018.
[39] Materials project website. [Online]. Available: https://www.materialsproject.org
[40] J. Castaing, R. Caudron, G. Toupance, and P. Costa, "Electronic structure of transition metal diborides," *Solid State Commun.*, vol. 7, pp. 1453–1518, 1969.
[41] R. M. Martin, *Electronic Structure: Basic Theory and Practical Methods*. Cambridge, U.K.: Cambridge Univ. Press, 2004.
[42] Quantumwise, Copenhagen, Denmark. *Atomistix software handbook.* [Online]. Available: http://www.qunatumwise.com
[43] A. Yariv, *Optical Electronics in Modern Communications*. New York, NY, USA: Oxford Univ. Press, 1997.
[44] J. Teyssier *et al.*, "Optical study of electronic and electron-phonon coupling in ZrB12," *Phys. Rev. B*, vol. 75, 2007, Art. no. 134503.
[45] L. Sartinska *et al.*, "Effect of concentrated light on morphology and vibrational properties of boron and tantalum mixtures," *Heliyon*, vol. 4, 2018, Art. no. e00585.
[46] F. Guinneton, L. Sauques, J. C. Valmalette, F. Cros, and J. R. Gavarri, "Comparative study between nanocrystalline powder and thin film of vanadium dioxide VO2: electrical and infrared properties," *J. Phys. Chem. Solids*, vol. 62, pp. 1229–1238, 2001.
[47] R. A. Nyquist and R. O. Kagel, *Infrared Spectra of Inorganic Compounds*. New York NY, USA: Academic Press, 1971.
[48] M. Curie *et al.*, "Quantifying pulsed laser induced damage to graphene," *Appl. Phys. Lett.*, vol. 99, 2011, Art. no. 211909.
[49] H. T. Hattori, A. Khaleque, L. Liu, and M. R. Greck, "Ytterbium-doped Q-switched fiber laser based upon manganese dioxide (MnO_2) saturable absorber," *Appl. Opt.*, vol. 55, pp. 9226–9231, 2016.
[50] J. J. Degnan, "Optimization of passively Q-switched lasers," *IEEE J. Quantum Electron.*, vol. 31, no. 11, pp. 1890–1901, Nov. 1995.